Controlling thermal stability and volatility of organogold(I) compounds for vapor deposition with complementary ligand design

Matthew B. E. Griffiths*†, Zachary S. Dubrawski†, Goran Bačić†, Jason D. Masuda‡, Achini Japahuge†, Tao Zeng†, and Seán T. Barry†

† Department of Chemistry, Carleton University, 1125 Colonel By Drive, Ottawa, Ontario, K1S 5B6, Canada

‡ Department of Chemistry, Saint Mary's University, Halifax, Nova Scotia, B3H 3C3, Canada

Abstract

Atomic layer deposition (ALD) of gold is being studied by multiple research groups, but to date no process using non-energetic co-reactants has been demonstrated. In order to access milder co-reactants, precursors with higher thermal stability are required. We set out to uncover how structure and bonding affect the stability and volatility of a family of twelve organogold(I) compounds with a combined X-ray diffraction (XRD), thermogravimetric analysis (TGA), differential scanning calorimetry (DSC), and density functional theory (DFT) investigation. Small, unsubstituted phosphonium ylide ligands bind more strongly to Au(I) than their silyl-substituted analogues, but their utility suffers due to their poor volatility and substantial thermal decomposition. Pentafluorophenyl (PFP^-) is introduced as a new, very electronegative ligand for gold vapor deposition precursors, and it was found that the penalty to volatility due to π-stacking and other intermolecular interactions in the solid state was overshadowed by dramatic improvements to kinetic and thermodynamic stability. We introduce a new figure of merit to compare and rank the suitability of these and other complexes as precursors for vapor deposition. Finally, DFT calculations on four compounds that have high figures of merit show a linear correlation between the gold-coordinative ligand bond dissociation energies and the observed decomposition temperatures, justifying this design strategy.

Introduction

Atomic layer deposition (ALD) is a chemical vapor deposition (CVD) technique that relies on specific surface chemistries to force growth into a self-limiting layer-by-layer regime.[1] Films deposited by ALD are highly conformal to substrate geometry, and subnanometer thickness control can be easily achieved by changing the number of sequential reactant exposures (i.e., cycles). Recently, two different ALD processes to deposit gold metal were reported using organogold(III) precursors: one by our group using oxygen-plasma and water as co-reagents, and the other by Mäkelä and co-workers using ozone.[2,3] While both processes were effective at depositing gold metal with high growth rates at low temperatures, they inherently suffer similar limitations in their scope. Firstly, thermal instability due to recombination of energetic oxygen species prevents high-degrees of uniformity of the thickness of the films down high-aspect ratio trenches, vias, or tortuous geometries.[4,5] Secondly, many substrates are incompatible with oxygen plasma or ozone and are therefore incompatible with these processes.

The strategy most often used for selecting viable compounds to use as new potential ALD precursors is to turn to previous literature; pick the best candidates based on volatility, thermal stability, and reactivity; and try to adapt them for use in an ALD process. While this was fruitful for

gold, as shown by both reported processes using previously reported CVD precursors,[6–8] this selection process only returns a handful of molecules that are often quite different from one another in their chemistry. ALD precursor design for other materials is quite mature in some cases and has been proven to be a useful tool in accelerating process development for Cu, Ru, Co, Ni, and many other metallic films.[9,10] As such, we felt that a thorough study on the fundamental factors that govern thermal stability and volatility would be useful in the development of new gold ALD precursors.

Many Au(I) CVD precursors decompose below 200°C.[11] By comparison, the current two ALD precursors undergo thermolysis at 140°C trimethylgold(III) trimethylphosphine (**A**) and 220°C dimethyl(diethyldithiocarbamato-κ^2-*S,S'*)gold(III) (**B**) (Scheme 1), which manifested in upper process temperatures being limited to 120 °C and 180 °C, respectively. We hypothesized that milder co-reagents than plasma or ozone could be used if higher temperatures could be accessed, therefore requiring precursors with higher thermal stability.

Scheme 1. Two previously reported precursors for gold ALD.

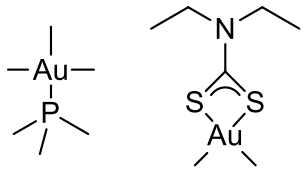

A **B**

This work reports a study of a family of potential gold(I) vapor deposition precursors based on a framework with interchangeable coordinative and anionic ligands to allow a systematic understanding not only of the steric and electronic effects of these ligands, but also of their cooperative effects on the volatility and thermal stability of the compound.

Alkylgold(I) phosphine compounds are known to decompose through a bimolecular reductive elimination pathway (Scheme 2). Trimethylphosphine methylgold(I) (**1a**) is reported to be stable as a neat liquid until 150°C, at which point dissociation of trimethylphosphine occurs followed by bimolecular reductive elimination of ethane gas.[12] However, on active metal surfaces this decomposition is known to occur as low as room temperature: the Au-PMe_3 bond dissociates on the surface, allowing bimolecular reductive elimination to take place.[13,14]

Scheme 2. Decomposition pathways for (PMe_3)AuMe as a neat liquid and in the presence of an active metal surface.

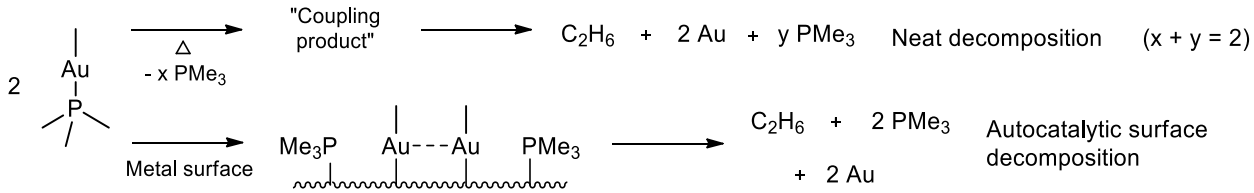

Given this, we focused on three complementary synthetic strategies to increase the thermal stability of Au(I) complexes. First, increasing the steric bulk of the anionic ligand should hinder the bimolecular reductive elimination pathway by preventing the association of adjacent surface-bound Au(I) species. Second, since the rate-limiting step of this reaction is dissociation of the coordinative phosphine ligand, a more electron-withdrawing anionic ligand should make the Au(I)

center more acidic, thus strengthening the bond of the coordinative ligand. Lastly, using coordinative ligands of other known thermally stable Au(I) complexes that have not been used for CVD may yield novel and useful ligand combinations, and reveal cooperative effects that further prevent thermolysis. Thus, we envisioned a family of compounds that would allow us to discover which factors conferred the most thermal stability to organogold(I) compounds (Chart 1).

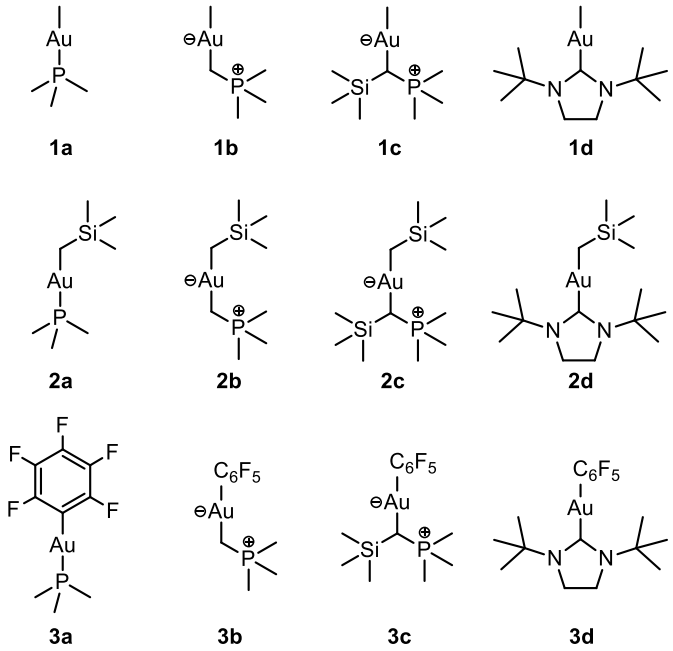

Chart 1. Family of Au(I) compounds considered in this study.

Starting from the known methylgold(I) CVD precursor **1a**, substituting trimethylsilylmethyl (NeoSi$^-$) and pentafluorophenyl (PFP$^-$) ligands should impart a stepwise increase in the overall thermal stability of the compound. NeoSi$^-$ is sterically bulkier and more electronically stabilizing than Me$^-$ (as well as neopentyl) due to low lying empty Si *d* orbitals. Both factors greatly increase the thermal stability of transition metal complexes bearing this ligand as was demonstrated by Wilkinson et al.[15,16] PFP$^-$ is sterically as bulky as NeoSi$^-$ (*vide infra*) but is much more σ-electron withdrawing due to perfluorination, which should result in a stronger coordinative bond to the gold center and increase the activation energy required for decomposition via bimolecular reductive coupling. PFP$^-$ complexes of gold with and without phosphine coordinative ligands have previously been shown to have high thermal stability, but have not been used for CVD or ALD.[17,18]

Phosphines are strongly binding coordinative ligands for organogold(I) compounds. Their chemistry is well known and predictable, the gold(I) compounds are stable to air and moisture, and are generally volatile.[19] We chose trimethylphosphine (PMe_3) as one of four neutral coordinative ligands (**1-3a**) due to its low molecular weight, ease of use in synthesis, and good *σ*-donation capabilities.

Schmidbaur and Franke reported “remarkably stable” organometallic gold(I) complexes bearing trimethylmethylene phosphorane (Ylide) and trimethyl(trimethylsilylmethylene) phosphorane (TMS-ylide) phosphonium ylides as neutral coordinative ligands.[19] These phosphonium ylides readily displace PMe_3 from **1a** and **2a** giving **1b,c** and **2b,c** which were reported to be more

thermally stable than the parent PMe_3 complexes (decomposing above 150 °C in the case of **1b**). Since phosphonium ylide compounds of Au(I) have to our knowledge not yet been tested for vapor deposition applications, and their volatilities have not been assessed, we included them and their PFP^- analogues in this study.

N-Heterocyclic carbenes (NHCs) have been successfully used by our group in the design of ALD precursors for copper metal, a CVD precursor for gold metal, and an ALD precursor for silver metal.[20–23] Their popularity in chemical literature following the seminal work of Arduengo[24,25] began with their propensity to act as drop-in improvements to phosphines for improved catalytic activity and stability.[26] Their ease of synthesis, structural and electronic diversity,[27,28] and greatly improved buried volume ($\%V_{bur}$)[29] distinguish them from phosphines. *N,N'*-di-*tert*-butylimidazolidin-2-ylidene[30] (NHC) is a monomeric, thermally stable, and sterically bulky saturated NHC with better *σ*-donor and *π*- acceptor properties than the more common imidazol-2-ylidene ligand class. This NHC should enhance the thermal stability of organogold(I) compounds due to its strong electron donating ability as well as its ability to sterically protect the Au(I) center.

Results and Discussion

Crystallography

Volatility is arguably the most important property of an ALD precursor as it sets the lower bounds of useable process temperatures. It is primarily dictated by intermolecular forces and, to a lesser extent, by the molecular weight of the compound. Since a compound's volatility can be readily determined by TGA, we sought to understand which intermolecular interactions affect volatility the most, thus single-crystal X-ray crystallography was used to determine the solid-state packing of **1c,d**, **2b,d,** and **3a,b,c,d** (Figure 1).

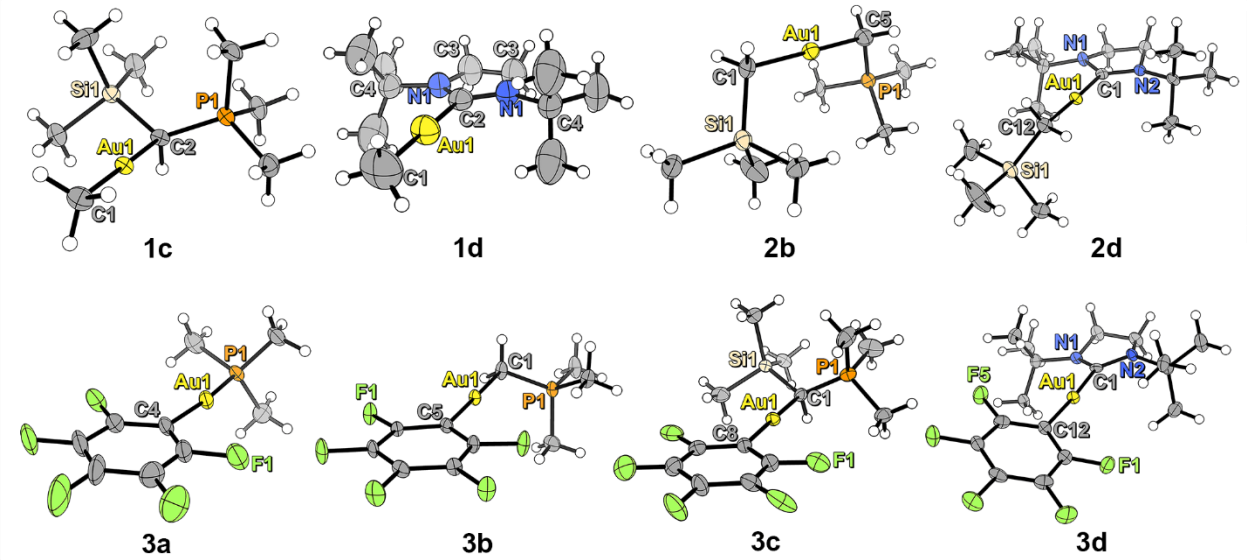

Figure 1. Solid-state structures of **1c**, **1d**, **2b**, **2d**, **3a**, **3b**, **3c**, and **3d**. In the cases of **1c** and **3c** only the *S* enantiomers are shown. Ellipsoids are drawn at 50 % probability in all diagrams.

Compound **1c** displayed Au-R (anionic ligand) and Au-L (neutral ligand) bond lengths of 2.057(3) Å and 2.136(3) Å, respectively. This compound, like its TMS-ylide derivative (**3c**), crystallizes as a 1:1 mixture of *R* and *S* enantiomers at the chiral ylidic carbon center coordinated to Au. The P-

C_{ylide} bond length is shorter than the mean P-Me bond length (1.742(3) Å vs. 1.793(9) Å respectively), and the P-C_{ylide}-Si angle (121.6(2)°) is much larger than expected for a tetrahedral geometry. These factors indicate that the bonding of this compound lies somewhere between it's two extreme canonical structures once complexed with gold (Scheme 3). Steric repulsion between the PMe_3 and $SiMe_3$ groups may influence the large angle and therefore hinder the σ-donating ability of this ligand. While the P-C_{ylide} bond length in the free ligand is not known, donation of electron density to a metal center would cause an elongation of this bond and result in a favouring of the ylidic resonance structure over the neutral species, which would elongate the P-C_{ylide} bond.

The structure of compound **1d** was collected at room temperature because the compound undergoes a phase transition near 77 K. This resulted in large thermal ellipsoids and no apparent intermolecular close contacts within the sum of the van der Waals radii. The Au-R and Au-L bond lengths of 2.069(8) Å and 2.055(6) Å are similar to both those of the known imidazole-2-ylidene derivative (2.063(4) Å and 2.044(3) Å)[31] and the other imidazolidin-2-ylidene compounds described here. The Au-Me bond length is slightly longer than that observed in **1c** (2.057(3) Å) which is consistent with a higher σ-donor ability (*trans*-effect) of the NHC. The NCN angle of the complexed NHC ligand (108.5(5) °) is slightly larger than that of the free NHC (106.44(9) °)[30] which is expected upon complexation to a Lewis-acidic metal center.

Scheme 3. Resonance structures depicting the extreme canonical resonance structures and ligand geometries of compounds 1,2,3c.

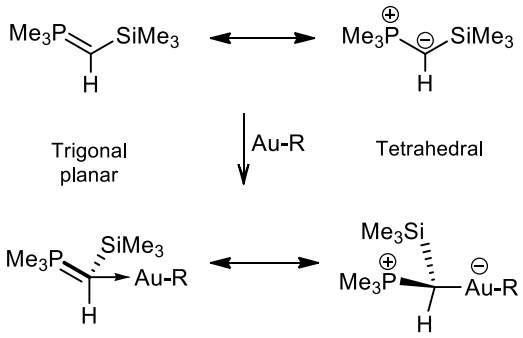

Table 1. Selected bond distances, angles, and buried volume values for the analyzed compounds

	R⁻	*L*	*Au-R (Å)*	*Au-L (Å)*	*P-C_{ylide} (Å)*	*Average P-Me (Å)*	*%V_{bur}*	*R-Au-L (°)*
1c	Me	TMS-ylide	2.057(3)	2.136(3)	1.742(3)	1.793(9)	53.7	178.1(1)
1d	Me	NHC	2.069	2.054	-	-	58.2	180
2b	NeoSi	Ylide	2.10(1)	2.09(1)	1.77(1)	1.80(4)	52.0	178.5(3)
2d	NeoSi	NHC	2.059(7)	2.045(7)	-	-	66.0	178.1(3)

3a	PFP	PMe_3	2.053(5)	2.280(1)	-	-	48.5	172.8(1)
3b	PFP	Ylide	2.046(3)	2.081()	1.763(3)	1.789(10)	51.8	177.9(1)
3c	PFP	TMS-ylide	2.041(3)	2.104(3)	1.759(3)	1.789(11)	61.5	178.4(1)
3d	PFP	NHC	2.039(4)	2.031(4)	-	-	66.0	176.7(1)

Compound **2b** displays Au-R and Au-L bond lengths of 2.10(1) Å and 2.09(1) Å. These comparatively long bond lengths are consistent with the strong trans effect of both ligands around the gold center. Acceptance of electron density from the ylidic carbon by the Au center is more pronounced here compared to **1c** due to the absence of the Me_3Si group on the ylide, as shown by the shorter Au-L bond. The P-C_{ylide} bond length is elongated compared to that of the free ylide (1.77(1) Å and 1.640(6) Å respectively)[32] due to donation of carbanionic character from the ylidic carbon to the lewis acidic Au center. Here, the P-C_{ylide} bond length not significantly different from the mean P-Me bond length (1.77(1) Å vs. 1.80(4) Å, respectively). This similarity distinguishes this system from the TMS-ylide **1c** as being primarily ylidic in nature.

Compound **2d** displays Au-R and Au-L bond lengths of 2.059(7) Å and 2.045(7) Å which are both slightly shorter than those found in **1d**. This implies a slightly more stable system, likely due to the decreased trans effect of $Me_3SiCH_2^-$ compared to Me^-. The NCN bond angle was 108.5(6)° which is similar to that of **1d**.

Compound **3a** displays Au-R and Au-L bond lengths of 2.053(5) Å and 2.280(1) Å, and a distorted R-Au-L bond angle of 172.8(1)° which is likely a low-energy deformation that allows a more stabilized crystalline network to form.[33] By comparison, the known PPh_3 analogue displays similar bond lengths (2.07(2) and 2.27(1) Å respectively) but has a more linear bond angle of 178(1)°.[34]

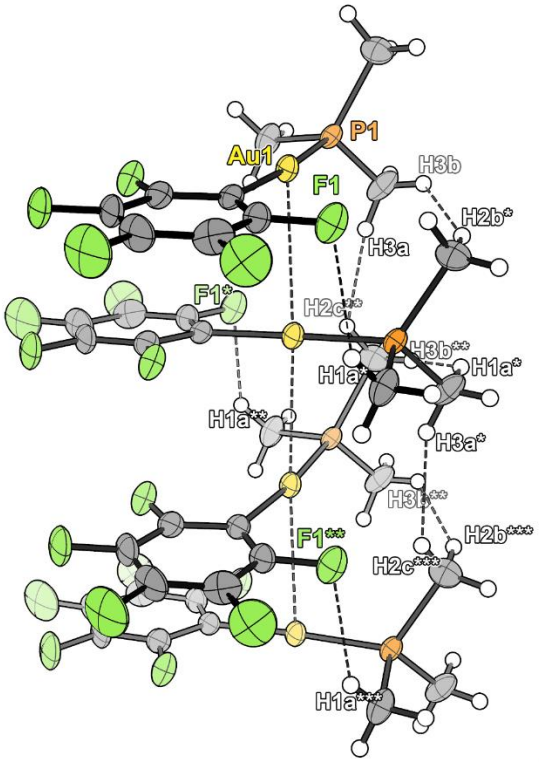

Figure 2. Extended structure of **3a** showing the aurophilic polymer chain. Thermal ellipsoids are shown at 50 % probability. Selected intermolecular interaction distances (Å): Au(1)-Au(2) 3.3703(6), H(1a***) – F(1**) 2.492, H(2c***) – F(1**) 2.527, H(2c***) – H(3a*) 2.319, H(2b***) – H(3b**) 2.343.

Compound **3a** packs as infinite chains where each molecule is rotated by roughly 90° from one another in an alternating fashion. Each molecule is associated to its neighbor by polymeric Au-Au aurophilic interactions (Au-Au distance 3.3703(6) Å). This was the only compound structurally characterized in this work that displayed aurophilicity (Figure 2). This is an intermediate-to-long range aurophilic interaction,[35] and is likely only observed for **3a** because PMe_3 is the least sterically bulky and most highly symmetrical coordinative ligand in this study. By comparison the previously reported PPh_3 analogue does not display aurophilic interactions, but instead undergoes a π-stacking interaction between the PFP^- ligands because the aurophilic interaction is inhibited by the steric bulk of the PPh_3 ligand.[34] In-chain intermolecular interactions are also facilitated by the PMe_3 ligand, each phosphine engages in three interactions to an adjacent molecule (H(1a***) - F(1**) 2.492 Å, H(2c***) – F(1**) 2.527 Å, H(2b***) – H(3b**) 2.343 Å) and one interaction to a molecule two units away in the chain H(2c***) – H(3a*) 2.319 Å. The aurophilic chains of **3a** are arranged in a columnar fashion with other chains (Figure S1) where each chain interacts with two adjacent chains. These stabilizing intermolecular interactions translate to a suppression of the volatility of **3a** compared to **1,2a**.

Compound **3b** displays the shortest Au-R and Au-L bond lengths (2.046(3) Å and 2.081(4) Å) of the phosphonium ylide compounds, which are indistinguishable from those of the known triphenylphosphonium ylide analogue.[36] The P-C_{ylide} bond is shorter than the average P–Me bond length (1.763(3) Å vs. 1.789(10) Å respectively), implying that there is more ylene character in this system than in **2b**. Compound **3b** is involved in a π-stacking interaction with one other molecule with a centroid to centroid distance of 3.497 Å. The π-stacked dimers interact with one another along the crystallographic *b x (a+c)* plane through F-F, C-F, and C-C interactions (Figure 3). The extensive intermolecular network formed by **3a** and **3b** shows that the addition of a PFP^- group introduces many more intermolecular interactions when coupled with a small ligand like PMe_3 or CH_2PMe_3 than with larger ligands like CH_2PPh_3.

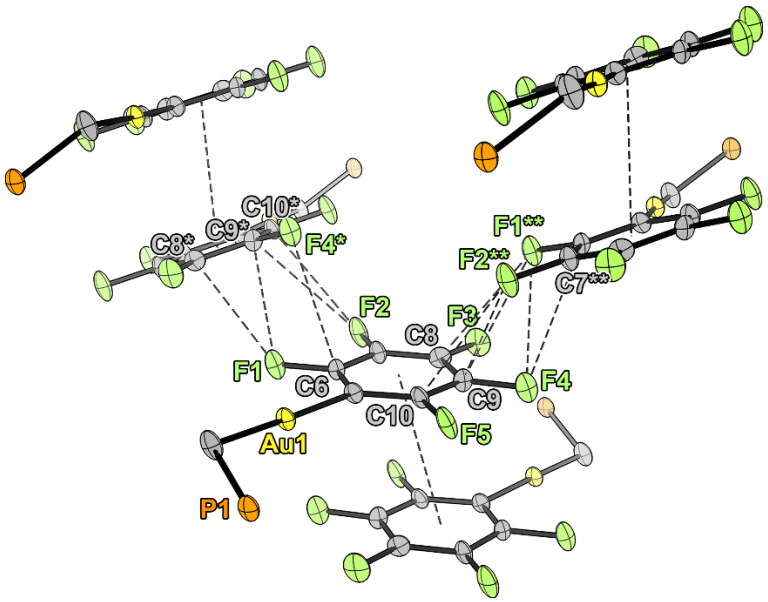

Figure 3. PFP – PFP intermolecular interactions in **3b**. The diagram displays pairs that occur along the crystallographic *b x (a+c)* plane. Methyl moieties of the ylide and hydrogen atoms have been omitted for clarity. Thermal ellipsoids are shown at 50 % probability. Selected intermolecular interaction distances (Å): centroid-to-centroid 3.497, F(2**) – C(10) 3.210(3), F(2**) – C(9) 3.166(3), C(7**) – F(4) 3.231(6), F(1**) – F(4) 2.928(2), F(1**) – C(9) 3.127(3), F(1**) – C(8) 3.145(3).

Compound **3c** displays Au-R and Au-L bond lengths of 2.041(3) Å and 2.104(3) Å respectively which are both shorter than its counterpart **1c** (2.057(3) Å and 2.136(3) Å respectively). The P-C_{ylide} bond length is shorter than the mean P-Me bond length (1.759(3) Å vs. 1.798(11) Å, respectively) and the P-C_{ylide}-Si angle (121.7(2)°) is large for an ideal tetrahedral geometry, all of which implies a significant ylene character. Compound **3c** does not π-stack in the solid state, instead the PFP^- ligands interact to form polymeric chains via (C-F)-F interactions that are comparatively much weaker than those observed in **3a,b** (Figure 4). This highlights the effectiveness of sterically bulky coordinative ligands in suppressing intermolecular interactions in PFP-Au complexes, and manifests as an increase in volatility in all TMSylide compounds compared to their analogous ylide compounds *vide infra*.

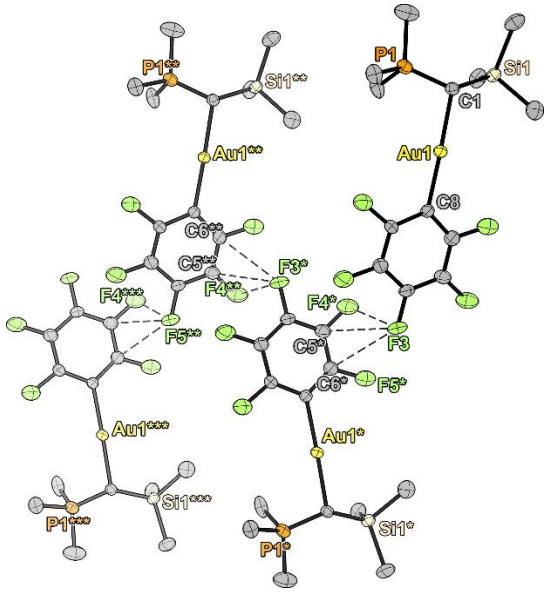

Figure 4. PFP – PFP intermolecular interactions in **3c**. Hydrogen atoms have been omitted for clarity and thermal ellipsoids have been drawn at the 50% probability level. The top two molecules are the (*S*) enantiomer while the bottom two are the (*R*) enantiomer. Selected intermolecular interaction distances (Å): F(3) – F(4*) 2.912(3), F(3) – C(2*) 3.151(4), F(3) – C(3*) 3.214(3).

Compound **3d** displays the shortest Au-R and Au-L bonds of the analyzed compounds (2.039(4) and 2.031(4) Å respectively). The compound also displays the largest deviation from the free ligand CNC angle (109.4(3)°) compared to 106.44(9)° respectively). This compound displays fewer overall intermolecular close contacts than **3b** and **3c** (Table 2) which we attribute to the large steric bulk of the NHC. The PFP^- ligand interactions are more suppressed than **3c**, where only a single pair of (C-C) – F p-π interactions (Figure 5) are allowed. By comparison, this PFP^- compound has a number of close contacts similar to its aliphatic analogue **2d**.

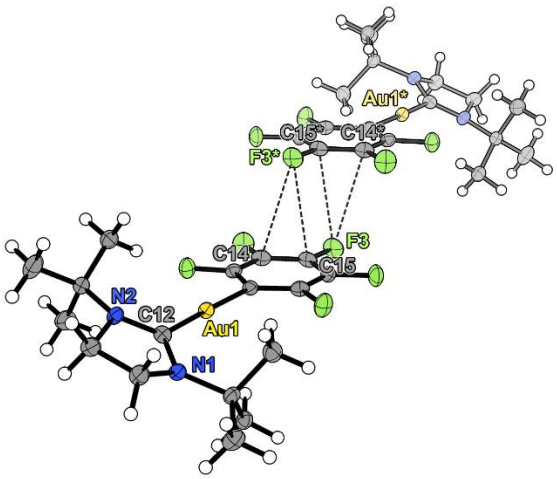

Figure 5. PFP – PFP intermolecular interactions in **3d**. Thermal ellipsoids have been drawn at the 50% probability level. Selected intermolecular interaction distances (Å): C(14) – F(3*) 3.095(4), C(15) – F(3*) 3.043(4).

When comparing R-Au bond lengths, PFP^- compounds all exhibit shorter bonds than other compounds with the same coordinative ligand: **1d ≈ 2d** > **3d**, **1c** > **3c**, and **2b** > **3b** (see Table 1). This is primarily due to the covalent radius of the sp^2-hybridized carbon in the PFP^- ring being slightly smaller than that of an sp^3-hybridized carbon. Furthermore, PFP^- complexes **3a-d** display shorter Au-L bond lengths than their aliphatic derivatives, which is due to the strong electron-withdrawing ability of the PFP^- ligand. This creates a more acidic metal center, which favours a stronger Lewis acid-base interaction with the coordinative ligand. Thus, crystallographic analysis suggested that PFP^- was an especially good ligand for improving the thermal stability of Au(I) compounds for two reasons. Firstly the rate-limiting step must proceed through cleavage of a stronger coordinative bond, and secondly because the final reductive elimination step must occur between two strongly bonded, electron-deficient carbon atoms.

Table 2. Tally of the number and type of intermolecular close-contacts observed in the solid-state structures of the analyzed compounds.[37,38]

	Number of intermolecular close-contacts								
	H-H	*C-H*	*C-C*	*F-H*	*F-C*	*F-F*	*Au-H*	*Au-Au*	*Total*
1c	4	2							6
1d									0
2b	2								2
2d	8	2							10
3a	4			8	2			2	16
3b			8	5	10	2	4		29
3c				8	4	2			14
3d		1		6	4				11

The range of an intermolecular close contact was defined as the sum of the van der Waals radii for the specific atom pairs. Van der Waals radii (Å): H (aliphatic) 1.2, C (aliphatic) 1.7, C (aromatic) 1.77, F (aromatic) 1.47. Au (1.66).

Complexes bearing Me^- (**1c,d**) or $NeoSi^-$ (**2b,d**) ligands display relatively few intermolecular contacts (Table 2). These compounds also do not display aurophilic interactions; they are exclusively interacting via weak van der Waals intermolecular interactions. Therefore, we expect the volatility of these complexes to be primarily influenced by their molecular weight. In stark contrast, the PFP^- complexes (**3a-d**) display far more intermolecular interactions in the solid state. We note that the highest number of interactions in the **3a-d** series is found for **3b**, whereas the less sterically hindered **3a** displays considerably fewer close contacts. The large number of contacts is due to the two-fold interaction of PFP^- ligands with neighboring π-stacked PFP^- dimers but is also reflective of the associative strength of the π-stacking interaction itself. It appears that the associative strength of the aurophilic interactions in **3a** dominates a weaker π-stacking system like in **3b**. This has the effect of greatly reducing the number of intermolecular interactions but does not necessarily mean that **3a** will be more volatile since the aurophilic interactions are quite strong.

Through comparison of the PFP-Au complexes, a correlation between the types and strengths of intermolecular interactions and the total $\%V_{bur}$ of the complex (Table 1) can be described.[39] When PMe_3 is used, the overall $\%V_{bur}$ of the complex (48.5 %) is small enough to allow aurophilic interactions. The stabilizing effects of the aurophilic chain motif are clearly more favourable than a π-stacking interaction since there is more than enough room for the π-stacking interaction in compound **3a**. The aurophilic interactions become frustrated by switching to the ylide ligand in **3b** ($\%V_{bur}$ = 51.8%) and thus the next most stabilizing interaction (π-stacking) is the only one observed. This interaction can be disrupted by the addition of a larger ligand such as $CH_2(PMe_3)$ in (**3b**, $\%V_{bur}$ = 51.8 %) or PPh_3 ($\%V_{bur}$ = 55.1), where in both cases only a π-stacking interaction is observed. If the $\%V_{bur}$ is increased further, as in **3c** ($\%V_{bur}$ = 61.5 %) the π-stacking interaction is disrupted and instead only a weakly interacting chain of F-F and C-F contacts is observed (Figure 6). Finally, with the addition of the NHC ligand (**3d**, $\%V_{bur}$ = 66.0 %), all extended PFP^- networks are disrupted and only a single-partner p-π interaction is observed between two PFP^- (Figure 7). The increase in $\%V_{bur}$ not only disrupts PFP^- intermolecular interactions, but also suppresses the overall total of intermolecular interactions in the PFP-Au series (Table 2).

Given this trend we hypothesize that aurophilic interactions would be expected for compounds with an overall $\%V_{bur} \leq 48.5$ (**3a**) in linear non-ligand exchanging organogold(I) systems such as those in the family studied here. Thus, we can predict which compounds in this family should exhibit aurophilic interactions by extrapolation of the average $\%V_{bur}$ values obtained for each ligand. As such, **1a** (V_{bur} = 41.0 ± 0.6) and **1b** (V_{bur} = 44.0 ± 0.8) fall well below the $\%V_{bur} \leq 48.5$ criteria, and **2a** (V_{bur} = 49.1 ± 0.4) is just above the limit of our suggested criteria. **2c** ($\%V_{bur}$ = 62.2 ± 0.4) is not expected to exhibit aurophilic interactions.

Thermolysis

For a compound to be a potential ALD candidate, high thermal stability and volatility are required. Thermogravimetric analysis (TGA) of a thermally stable and volatile compound shows an exponential mass loss with constantly increasing temperature as described by the Clausius-Clapeyron equation. Thermally stable compounds will also leave a very low final residual mass which is indicative of evaporation without decomposition to non-volatile by-products like metallic gold. A compound's volatility can be inferred from the onset of its mass loss, but a better evaluation uses its vapor pressure which can be estimated from the derivative of the mass loss curve.[40] The temperature at which a compound achieves a vapor pressure of 1 Torr (i.e., its 1 Torr Temperature, T_V) may be used as a quantitative benchmark since commercial ALD reactors

typically operate close to this pressure (Figures S38-S45). Differential scanning calorimetry (DSC) complements TGA analysis by providing a thermodynamic onset of decomposition of the sample. By graphically determining the point at which the decomposition exotherm has reached 5 % of it's maximum height, we can obtain a decomposition temperature (T_D) for the compound in question (Figures S46-S57). The results of this analysis for the compounds evaluated here are tabulated below (Table 3).

Table 3. Important metrics obtained from TGA and DSC.

	T_V (°C)	*T_D (°C)*	*Useful temperature range (°C)*[a]	*Residual mass (%)*	*Fractional Gold remaining (%)*	*Figure of Merit (σ)*[b]	*$\Delta H_{vap/sub}$*[c]
1a	67.54 ± 0.01	130	62.5	34.3	50.2	31.1	65.72 ± 0.01
1b	-	107	-	22.9	35.1	-	-
1c	-	129	-	36.9	70.1	-	-
1d	156.8 ± 0.4	189	32.5	34.9	69.9	9.8	91.1 ± 0.2
2a	87.2 ± 0.2	146	59.1	0.8	1.5	58.2	59.6 ± 0.1
2b	-	152	-	2.5	4.8	-	-
2c	134.3 ± 1.0	118	-16.8	5.9	13.4	-14.6	60.5 ± 0.3
2d	150.6 ± 0.3	184	33.1	11.9	28.2	23.8	64.0 ± 0.1
3a	152.3 ± 0.5	185	33.1	1.1	2.5	32.3	75.4 ± 0.2
3b	-	220	-	41.3	95.2	-	-
3c	148.0 ± 1.5	253	104.7	33.3	88.8	11.7	44.7 ± 0.4
3d	200.3 ± 0.1	300	99.7	1.6	4.4	95.3	78.92 ± 0.04

[a] Difference between T_V and T_D. [b] See Equation 1. [c] Obtained from Clausius-Clapeyron curves which were derived from derivative curves of the TGA ramp data (Figure S2).[40] Dashes indicate that insufficient mass loss data could be obtained before the measured self-decomposition temperature of that compound.

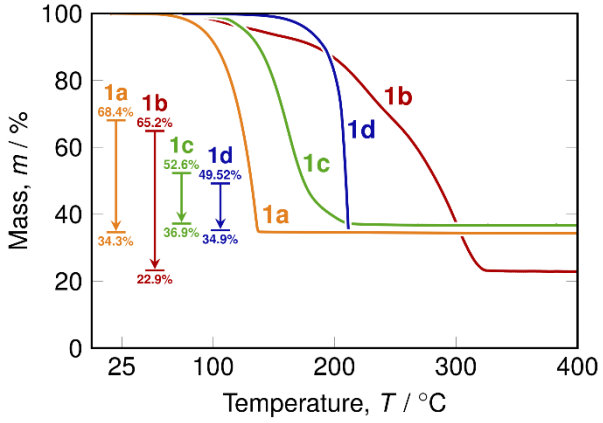

Figure 6. TGA of **1a-d** at a ramp rate of 10 °C/min. The vertical ranges show the % mass of Au in each compound (top line) and the final residual mass of the respective analysis. The inset

diagram shows the % mass of Au in the compound (top line) and the final residual mass of the respective analysis.

In the TGA ramp experiments of **1a-d** (Figure 6), none of the compounds were thermally stable enough to evaporate completely. All sample pans were left with a visibly golden coating after the experiments, thus the difference between top and bottom lines of the inset are indicative of how many of the gold atoms evaporated as gas-phase species. Compounds **1a** and **1d** show concurrent evaporation and decomposition. The fractional gold content remaining after thermolysis was 50 % and 70 % respectively, which indicates that some of the gold in these samples must have evaporated as a molecular species. From differential scanning calorimetry (DSC) we found that the respective onsets of self-decomposition for these two compounds were 130 °C and 189 °C, so a residual mass past these temperatures is expected.

In the case of **1a** it is interesting that such a high residual mass is observed, given that the self-decomposition point (130 °C) is close to the end of the mass loss curve. This can be explained by the known autocatalytic decomposition of alkylgold(I) phosphines that occurs as low as room temperature on Cr, Cu and Au surfaces.[13] Some decomposition likely occurs on the Pt surface of the pan at temperatures below the onset of thermolysis which increases residual mass. This occurs more readily for the phosphine than for the NHC which implies a strong NHC–Au(0) bond, possibly in a self-assembled monolayer-type fashion.[41] No inflection is observed in the exponential mass loss curves of **1a** and **1d** which suggests that the decomposition products are gaseous or non-volatile (i.e., metallic gold), and therefore their production does not affect the mass loss rate of the sample.

In the case of compounds **1b** and **1c**, concurrent evaporation and decomposition are clearly observed by the multiple inflection points in their respective mass loss curves. Here the thermolysis products formed are semi-volatile or are themselves thermally unstable. This makes the by-products observable as changes to the mass loss rate, implying low-volatility organic molecules or other gold complexes are the primary decomposition products of **1b** and **1c**. In the case of **1b**, at least one, and possibly all of the products are somewhat volatile judging from the fractional gold content remaining (35% of initial) which is the lowest of the methyl series. Compound **1c** appears to undergo a single thermolysis event, the products of which then lose mass more slowly until reaching a final residual mass of 36.9% (fractional gold remaining 70.1%). As with the other phosphonium ylide compounds *vide infra*, we suspect that these compounds decompose by a different mechanism than the phosphine or NHC complexes due to the multiple thermal events that occur upon heating.

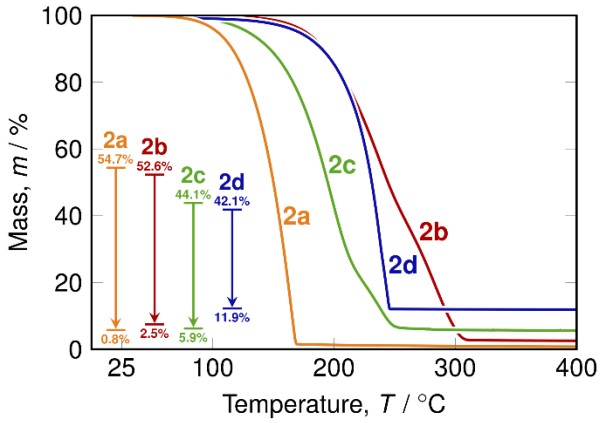

Figure 7. TGA ramp experiments of **2a-d** at a ramp rate of 10 °C/min. The inset diagram shows the % mass of Au in the compound (top line) and the final residual mass of the respective analysis.

NeoSi^{-} gold(I) compounds **2a-d** performed much better overall by TGA than their methylgold(I) counterparts (Figure 7). Compound **2a** appears to evaporate very cleanly, the only indication of slight decomposition being the small residual mass of 0.8 %. Compound **2d** evaporates with decomposition in a single step to 11.9 % (28.2 % Au remaining). The measured onsets of decomposition for these compounds by DSC (146 °C and 184 °C respectively) are similar to those of **1a** and **1d**. It is likely that the autocatalytic decomposition reactions of NeoSi-gold(I) species on platinum are kinetically slower than those of methylgold compounds, supporting the hypothesis that sterically bulkier ligands hinder thermolysis. This allows the compounds to persist to relatively higher temperatures and therefore evaporate more completely before kinetic decomposition can be observed.

Compounds **2b** and **2c** mirror their methylgold(I) counterparts and both undergo thermal decomposition to non-volatile species. In the case of **2b** two thermolysis events take place producing other volatile gold-containing species, leaving a small residual mass of 2.5 % (4.8 % Au remaining). Compound **2c** also appeared to undergo two sequential thermolyses, leaving a low residual mass of 5.9 % (13.4 % Au remaining). By comparison to **1b** and **1c** it is obvious that the NeoSi^{-} ligand improves the performance of the species by TGA, but not by increasing the thermal stability of the starting compounds. The onsets of decomposition of **1b** (107 °C), **1c** (129 °C), **2b** (152 °C), and **2c** (118 °C) were measured by DSC, and in every case these species begin to decompose before any real evaporation occurs in the TGA. We attribute the lower residual mass here to a difference in the by-products of thermal decomposition of **2b** and **2c** in comparison to their methylgold(I) counterparts.

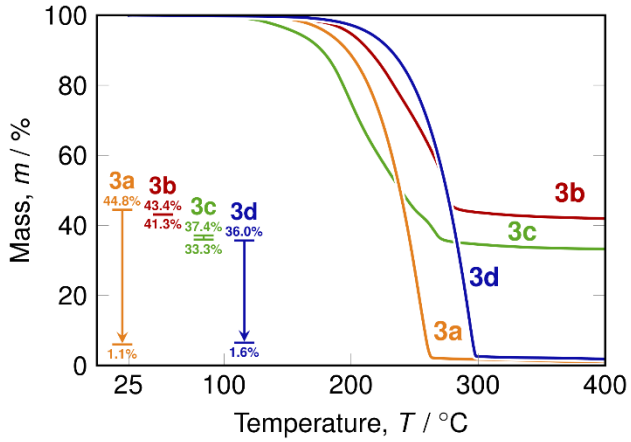

Figure 8. TGA ramp experiments of **3a-d** at a ramp rate of 10 °C/min. The inset diagram shows the % mass of Au in the compound (top line) and the final residual mass of the respective analysis.

The PFP^- compounds **3a** and **3d** performed well by TGA (Figure 8), evaporating in single steps and leaving very low residual masses (**3a**: 1.1 %, 2.5 % Au remaining; **3d**: 1.6 %, 4.4 % Au remaining, respectively). Volatilization occurs at higher temperatures for these species compared to their $NeoSi^-$ and Me^- counterparts, but the NHC compound **3d** in particular shows a marked improvement in its thermal stability compared to the other NHC compounds. Clearly PFP^- greatly stabilizes gold(I) and improves the thermal stability of the system at the expense of volatility.

Compounds **3b** and **3c** performed worse than their Me^- and $NeoSi^-$ counterparts, undergoing multiple thermolysis events that both ended with fractional gold residues above 85%. The introduction of the PFP^- ligand does improve thermal stability given the increases in the measured onsets of self-decomposition of these compounds (Table 3) but, in the case of **3b** and **3c,** the reduction in volatility is too great to result in a useful precursor. It is interesting to note that while **3b** begins self-decomposition at 220 °C, close to the onset of its mass loss by TGA, **3c** begins self-decomposition at 253 °C which is almost near the end of its mass loss by TGA. This implies that **3c** undergoes a more rapid decomposition than **3b** during the TGA analysis. It is unlikely that autocatalytic surface decomposition is the cause for decomposition of **3c** as in **1a** because the proposed by-products decafluorobiphenyl and trimethylsilyl(trimethylmethylene)phosphorene are both volatile and should result in a near-exponential mass loss, which was not observed.

From the thermal data collected, we defined a figure of merit (σ) to compare the viability of these compounds for use in vapor deposition processes (Equation 1). This figure of merit is made up of thermodynamic and kinetic terms that together describe the suitability of the vapor deposition precursor. Not only does it include decomposition temperature and vapor pressure, but if two compounds that both undergo the same decomposition mechanism are compared, the one which resists decomposition longer will receive a higher figure of merit. Although all species were shown to decompose by DSC before they reach a rest mass by TGA, some are more kinetically stable (e.g. **2a, 3a**) than others (e.g. **1a**). Particularly, **3a** far exceeds its onset of self-decomposition (185 °C), leaving only a 3% residual mass at 260 °C. This kinetic stability allows **3a** to resist bimolecular reductive elimination much longer than **1a** or **2a.** Thus, weighting the figure of merit by the residual mass demonstrates the importance of kinetic and thermodynamic stability of a potential precursor compound.

Equation 1. Figure of merit equation for vapor deposition precursor usefulness.

$$\sigma = (T_D - T_V) \times \left(1 - \frac{\%m_{res}}{196.97/_{MW} \times 100\%}\right)$$

The calculated σ values for the family of compounds are included in Table 3. Certain compounds (**1b, 1c**, **2b**, **3b**) were not given a σ value because insufficient mass loss data could be obtained before the TGA experiment reached the self-decomposition temperature (DSC) of the analyte in question. The merits of each compound in this family can be visualized using a "minefield" diagram (Figure 9). Since the delivery temperature of a precursor is an unavoidable consideration in process design, each circle is centered at the compound's respective T_V. If delivery temperature is not an issue, then clearly compound **3d** is the most promising precursor candidate for vapor deposition. It has a T_V of 200 °C however, so if only lower delivery temperatures are desired **2a** is likely the preferred candidate.

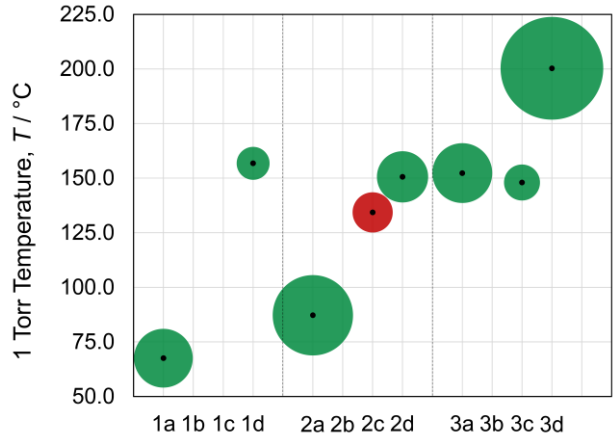

Figure 9. Figure of merit "minefield" diagram. Green circles indicate a positive figure of merit while red circles indicate a negative figure of merit. The σ value of each compound is shown as the radius of each circle in arbitrary units.

DFT study

To better understand the reason behind the high figure of merit obtained for phosphine and NHC systems, we undertook a density functional theory (DFT) study of compounds **2a,d** and **3a,d**. The calculations were first performed using model compounds **2a***, **2d***, **3a***, and **3d*** where the PMe_3 and NHC ligands were replaced with proto analogues (PH_3 and N,N'-dihydroimidazolidin-2-ylidene (H_2-NHC), to examine the energy required to break the Au-R and Au-L bonds. All calculations were carried out using the ωB97X-D functional[42,43] and the iMCP-SR2 model core potentials and basis sets.[44] Scalar-relativistic model core potentials are known to provide satisfactory description for heavy elements like Au.[45] The dissociation energies of the R^- and L ligand fragments were determined by calculating the difference in energy between the free ligand in question and the remaining Au-L or Au-R fragment. Three scenarios were considered: dissociation of the coordinative ligand, forming a neutral R-Au fragment and a neutral L fragment;

homolytic cleavage of the R-Au bond resulting in R• and •Au-L fragments; and heterolytic cleavage of the R-Au bond resulting in R^- and $^+$Au-L fragments (Table 4). Heterolytic cleavage was discounted after considering the results of **3a*** and **3d***, because it was consistently the highest energy case and was therefore unlikely to contribute to the first thermolysis events of the molecules. For **2a,d** and **3a,d** only dissociation of the neutral L ligand was considered since it was known to be the primary decomposition pathway for alkylgold(I) compounds. It was also the lowest energy case, implying it was the largest contributor to thermal decomposition.

Table 4. Calculated energies and measured decomposition temperatures of the three ligand dissociation cases for model compounds and synthesized compounds.

Compound	*Dissociation of coordinative ligand (kJ/mol)*	*Homolytic cleavage (kJ/mol)*	*Heterolytic cleavage (kJ/mol)*	*T_d (°C)*[a]
NeoSi-Au-PH_3 (**2a***)	119	293	-	-
NeoSi-Au-PMe_3 (**2a**)	171	-	-	145
NeoSi-Au-H_2NHC (**2d***)	215	452	-	-
NeoSi-Au-^{t}BuNHC (**2d**)	221	-	-	184
PFP-Au-PH_3 (**3a***)	153	422	727	-
PFP-Au-PMe_3 (**3a**)	212	-	-	185
PFP-Au-H_2NHC (**3d***)	263	593	665	-
PFP-Au-^{t}BuNHC (**3d**)	277	-	-	300

[a] Onset of self-decomposition as measured by DSC.

The model compounds **2a***, **2d***, **3a***, and **3d*** mirrored the general trends of thermal stability that were observed experimentally for their respective synthetic ligands. The energy required for homolytic R-Au bond cleavage increased from $NeoSi^-$ to PFP^- which reflects the tendency for PFP^- ligands to resist reductive elimination. Exchanging PH_3 for H_2-NHC resulted in an increase in both Au-L dissociation energy and R-Au homolytic bond cleavage energy, which is due to the relatively higher electron donating ability of the NHC ligand. Au-L bond dissociation energies increased from $NeoSi^-$ to PFP^- and from PMe_3 to NHC which is reflective of the σ-withdrawing capability of the PFP^- ligand as well as the increased σ-donor ability of the NHC compared to PMe_3.

Compounds **2a** and **3a** show significantly higher Au-L bond dissociation energy than **2a*** and **3a*** since PH_3 is a much worse σ-donor than PMe_3 due to the electron donating Me groups being directly bound to the ligating atom (P). The change in N-substituents in the NHC compounds has comparatively little effect on the Au-L bond strength since the alkyl group is relatively remote from the ligating C atom. **2d*** and **3d*** were calculated to have Au-L bond dissociation energies that were comparable to **2d** and **3d**.

Thermal stability observed by DSC correlates well to the calculated Au-L bond dissociation energies (Figure 10). Since the decomposition of these compounds is known to proceed via the rate-limiting step of Au-L bond dissociation, a linear correlation between the observed

decomposition temperature and the calculated Au-L bond dissociation energy is expected and is observed for these compounds. The calculational and TGA results corroborate each other.

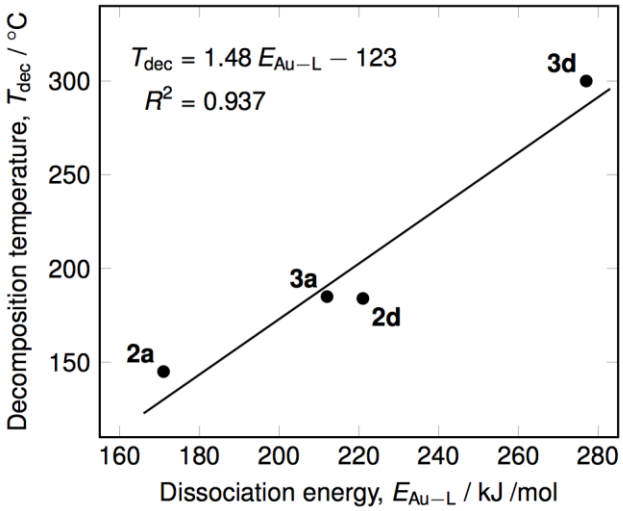

Figure 10. Correlation between *ab initio*-calculated Au-L bond dissociation energies and the observed self-decomposition temperatures for **2a,d, 3a,d**.

Being able to predict a compound's thermal stability from ligand choice is a useful tool that allows for rational design and theoretical evaluation of different ligand classes before undertaking synthesis and testing. Furthermore, for a single type of ligand, if the nature of alkyl groups has little effect on the overall thermal stability of the compound (such as **3d*** ≈ **3d**) then these alkyl groups can be repurposed to introduce volatility or other desirable properties upon the potential precursor. The implementation of this strategy is of ongoing interest to us in the further development of vapor deposition precursors for Au and other metals.

Conclusions

A family of 12 gold(I) compounds were synthesized and analyzed for their use as precursors for gold metal vapor deposition applications. Single crystal x-ray diffraction was used to structurally characterize 8 of these compounds to assess the effect of the anionic and coordinative ligands on intermolecular interactions. Compounds with Me^- and $NeoSi^-$ ligands displayed fewer intermolecular interactions than those with PFP^- ligands due to the ability of the latter to undergo π-stacking and p-π interactions. **3a** undergoes aurophilic interactions due to its small % buried volume compared to the other structurally characterized compounds. Ylide compounds show more intermolecular interactions than TMS-ylide compounds, which is observable as an increase in volatility of the latter. TGA and DSC were used to assess the volatility and thermal stability of the family of compounds, and it was found that $NeoSi^-$ provides higher kinetic stability than Me^-. NHC and PFP^- ligands provide substantially higher thermodynamic stability to the gold(I) center, but hinder volatility. To deconvolute these effects we derived a figure of merit with which the viability of all gold(I) compounds may be compared for vapor deposition. **3d** has the highest merit, but is only useful at high delivery temperatures, while **2a** is most suitable for lower delivery temperature applications. Finally, using DFT we compared the calculated Au-L bond strength to

the measured onset of self-decomposition of four of the best performing compounds and found a linear correlation. In future studies, using this computational method for the design of vapor deposition precursors should inform the process of potential candidates prior to undertaking chemical synthesis.

References

(1) Miikkulainen, V.; Leskelä, M.; Ritala, M.; Puurunen, R. L. Crystallinity of Inorganic Films Grown by Atomic Layer Deposition: Overview and General Trends. *J. Appl. Phys.* **2013**, *113* (2).

(2) Griffiths, M. B. E.; Pallister, P. J.; Mandia, D. J.; Barry, S. T. Atomic Layer Deposition of Gold Metal. *Chem. Mater.* **2016**, *28* (1), 44–46.

(3) Mäkelä, M.; Hatanpää, T.; Mizohata, K.; Räisänen, J.; Ritala, M.; Leskelä, M. Thermal Atomic Layer Deposition of Continuous and Highly Conducting Gold Thin Films. *Chem. Mater.* **2017**, *29* (14), 6130–6136.

(4) Profijt, H. B.; Potts, S. E.; van de Sanden, M. C. M.; Kessels, W. M. M. Plasma-Assisted Atomic Layer Deposition: Basics, Opportunities, and Challenges. *J. Vac. Sci. Technol. A Vacuum, Surfaces, Film.* **2011**, *29* (5), 050801.

(5) Knoops, H. C. M.; Elam, J. W.; Libera, J. A.; Kessels, W. M. M. Surface Loss in Ozone-Based Atomic Layer Deposition Processes. *Chem. Mater.* **2011**, *23* (9), 2381–2387.

(6) Puddephatt, R. J.; Treurnicht, I. Volatile Organogold Compounds [AuR(CNR1)]: Their Potential for Chemical Vapor Deposition of Gold. *J. Organomet. Chem.* **1987**, *319* (1), 129–137.

(7) Messelhäuser, J.; Flint, E. B.; Suhr, H. Laser Induced CVD of Gold Using New Precursors. *Appl. Surf. Sci.* **1992**, *54*, 64–68.

(8) Parkhomenko, R. G.; Trubin, S. V.; Turgambaeva, A. E.; Igumenov, I. K. Deposition of Pure Gold Thin Films from Organometallic Precursors. *J. Cryst. Growth* **2015**, *414*, 143–150.

(9) Bernal Ramos, K.; Saly, M. J.; Chabal, Y. J. Precursor Design and Reaction Mechanisms for the Atomic Layer Deposition of Metal Films. *Coord. Chem. Rev.* **2013**, *257* (23–24), 3271–3281.

(10) Gordon, P. G.; Kurek, A.; Barry, S. T. Trends in Copper Precursor Development for CVD and ALD Applications. *ECS J. Solid State Sci. Technol.* **2014**, *4* (1), N3188–N3197.

(11) Baum, T. H.; Comita, P. B. Chemical Vapor Deposition of Gold and Silver. In *The Chemistry of Metal CVD*; Kodas, T. T., Hampden-Smith, M. J., Eds.; Wiley-VCH Verlag GmbH: Weinheim, Germany, 1994; pp 303–327.

(12) Tamaki, A.; Kochi, J. K. Formation and Decomposition of Alkyl-Gold(I) Complexes. *J. Organomet. Chem.* **1973**, *61*, 441–450.

(13) Holl, M. M. B.; Seidler, P. F.; Kowalczyk, S. P.; McFeely, F. R. Surface Reactivity of Alkylgold(I) Complexes: Substrate-Selective Chemical Vapor Deposition of Gold from RAuP(CH3)3 (R = CH2CH3, CH3) at Remarkably Low Temperatures. *Inorg. Chem.* **1994**, *33* (3), 510–517.

(14) Jansen, F.; Kruck, T. Promising New Precursors for the CVD of Gold. *Adv. Mater.* **1995**, *7*

(3), 297–300.

(15) Mowat, W.; Shortland, A.; Yagupsky, G.; Hill, N. J.; Yagupsky, M.; Wilkinson, G. Elimination Stabilized Alkyls. Part I. Chromium, Molybdenum, Tungsten, and Vanadium. *J. Chem. Soc. Dalt. Trans.* **1972**, No. 4, 533.

(16) Wozniak, B.; Ruddick, J. D.; Wilkinson, G. Trimethylsilylmethyl Complexes of Transition Metals with π-Bonding Ligands. *J. Chem. Soc. A Inorganic, Phys. Theor. Chem.* **1971**, No. 31, 3116–3120.

(17) Vaughan, L. G.; Sheppard, W. A. Organogold Chemistry II. Tris(Pentafluorophenyl)Gold(III). *J. Organomet. Chem.* **1970**, *22* (3), 739–742.

(18) Usón, R.; Laguna, A.; Laguna, M.; Usón, A. A New Route for the Synthesis of Gold(I) and Gold(II) Pentafluorophenyl(Ylide) Complexes. *Inorganica Chim. Acta* **1983**, *73* (C), 63–66.

(19) Schmidbaur, H.; Franke, R. Organogold-Chemie, XV. Gold(I)-Verbindungen Einfacher Phosphor-Ylide. *Chem. Ber.* **1975**, *108* (4), 1321–1328.

(20) Coyle, J. P.; Dey, G.; Sirianni, E. R.; Kemell, M. L.; Yap, G. P. A.; Ritala, M.; Leskelä, M.; Elliott, S. D.; Barry, S. T. Deposition of Copper by Plasma-Enhanced Atomic Layer Deposition Using a Novel N-Heterocyclic Carbene Precursor. *Chem. Mater.* **2013**, *25* (7), 1132–1138.

(21) Coyle, J. P.; Sirianni, E. R.; Korobkov, I.; Yap, G. P. A.; Dey, G.; Barry, S. T. Study of Monomeric Copper Complexes Supported by N - Heterocyclic and Acyclic Diamino Carbenes. *Organometallics* **2017**, *35*, 2800–2810.

(22) Griffiths, M. B. E.; Koponen, S. E.; Mandia, D. J.; McLeod, J. F.; Coyle, J. P.; Sims, J. J.; Giorgi, J. B.; Sirianni, E. R.; Yap, G. P. A.; Barry, S. T. Surfactant Directed Growth of Gold Metal Nanoplates by Chemical Vapor Deposition. *Chem. Mater.* **2015**, *27* (17), 6116–6124.

(23) Boysen, N.; Hasselmann, T.; Karle, S.; Rogalla, D.; Theirich, D.; Winter, M.; Riedl, T.; Devi, A. An N-Heterocyclic Carbene Based Silver Precursor for Plasma-Enhanced Spatial Atomic Layer Deposition of Silver Thin Films at Atmospheric Pressure. *Angew. Chemie Int. Ed.* **2018**, *57* (49), 16224–16227.

(24) Arduengo, A. J.; Harlow, R. L.; Kline, M. A Stable Crystalline Carbene. *J. Am. Chem. Soc.* **1991**, *113* (1), 361–363.

(25) Arduengo, A. J.; Dias, H. V. R.; Harlow, R. L.; Kline, M. Electronic Stabilization of Nucleophilic Carbenes. *J. Am. Chem. Soc.* **1992**, *114* (14), 5530–5534.

(26) Nolan, S. P. The Development and Catalytic Uses of N-Heterocyclic Carbene Gold Complexes. *Acc. Chem. Res.* **2011**, *44* (2), 91–100.

(27) Nelson, D. J.; Nolan, S. P. Quantifying and Understanding the Electronic Properties of N-Heterocyclic Carbenes. *Chem. Soc. Rev.* **2013**, *42* (16), 6723.

(28) Munz, D. Pushing Electrons - Which Carbene Ligand for Which Application? *Organometallics* **2018**, *37* (3), 275–289.

(29) Clavier, H.; Nolan, S. P. Percent Buried Volume for Phosphine and N-Heterocyclic Carbene Ligands: Steric Properties in Organometallic Chemistry. *Chem. Commun.* **2010**,

46 (6), 841.

(30) Denk, M. K.; Thadani, A.; Hatano, K.; Lough, A. J. Steric Stabilization of Nucleophilic Carbenes. *Angew. Chemie Int. Ed. English* **1997**, *36* (23), 2607–2609.

(31) Baker, M. V.; Barnard, P. J.; Brayshaw, S. K.; Hickey, J. L.; Skelton, B. W.; White, A. H. Synthetic, Structural and Spectroscopic Studies of (Pseudo)Halo(1,3-Di-Tert-Butylimidazol-2-Ylidine)Gold Complexes. *Dalt. Trans.* **2005**, No. 1, 37.

(32) Ebsworth, E. A. V.; Fraser, T. E.; Rankin, D. W. H. The Molecular Structure of Trimethyl(Methylene)Phosphorane in the Gas Phase, Determined by Electron Diffraction. *Chem. Ber.* **1977**, *110* (11), 3494–3500.

(33) Veinot, A. J.; Todd, A. D. K.; Robertson, K. N.; Masuda, J. D. A Reinvestigation of Mono- and Bis-Ethynyl Phosphonium Salts: Structural and Computational Studies and New Reactivity. *Can. J. Chem.* **2018**, *96* (1), 8–17.

(34) Baker, R. W.; Pauling, P. J. Crystal Structure of (Pentafluorophenyl)(Triphenylphosphine)Gold(I). *J. Chem. Soc. Dalt. Trans.* **1972**, No. 20, 2264.

(35) Schmidbaur, H.; Schier, A. Aurophilic Interactions as a Subject of Current Research: An up-Date. *Chem. Soc. Rev.* **2012**, *41* (1), 370–412.

(36) Fernández, E. J.; Hardacre, C.; Laguna, A.; Lagunas, M. C.; López-de-Luzuriaga, J. M.; Monge, M.; Montiel, M.; Olmos, M. E.; Puelles, R. C.; Sánchez-Forcada, E. Multiple Evidence for Gold(I)···Silver(I) Interactions in Solution. *Chem. - A Eur. J.* **2009**, *15* (25), 6222–6233.

(37) Bondi, A. Van Der Waals Volumes and Radii. *J. Phys. Chem.* **1964**, *68* (3), 441–451.

(38) Schmidbaur, H. The Aurophilicity Phenomenon: A Decade of Experimental Findings, Theoretical Concepts and Emerging Applications. *Gold Bull.* **2000**, *33* (1), 3–10.

(39) Falivene, L.; Credendino, R.; Poater, A.; Petta, A.; Serra, L.; Oliva, R.; Scarano, V.; Cavallo, L. SambVca 2. A Web Tool for Analyzing Catalytic Pockets with Topographic Steric Maps. *Organometallics* **2016**, *35* (13), 2286–2293.

(40) Kunte, G. V.; Shivashankar, S. A.; Umarji, A. M. Thermogravimetric Evaluation of the Suitability of Precursors for MOCVD. *Meas. Sci. Technol.* **2008**, *19* (2), 025704.

(41) Crudden, C. M.; Horton, J. H.; Ebralidze, I. I.; Zenkina, O. V.; McLean, A. B.; Drevniok, B.; She, Z.; Kraatz, H. B.; Mosey, N. J.; Seki, T.; et al. Ultra Stable Self-Assembled Monolayers of N-Heterocyclic Carbenes on Gold. *Nat. Chem.* **2014**, *6* (5), 409–414.

(42) Chai, J.-D.; Head-Gordon, M. Systematic Optimization of Long-Range Corrected Hybrid Density Functionals. *J. Chem. Phys.* **2008**, *128* (8), 084106.

(43) Chai, J.-D.; Head-Gordon, M. Long-Range Corrected Hybrid Density Functionals with Damped Atom–atom Dispersion Corrections. *Phys. Chem. Chem. Phys.* **2008**, *10* (44), 6615.

(44) Lovallo, C. C.; Klobukowski, M. Development of New Pseudopotential Methods: Improved Model Core Potentials for the First-Row Transition Metals. *J. Comput. Chem.* **2003**, *24* (9), 1009–1015.

(45) Zeng, T.; Klobukowski, M. New Model Core Potentials for Gold. *J. Chem. Phys.* **2009**,

130 (20), 204107.